Analysis of Multipactor Effect in Coaxial Lines

A. Sounas, E. Sorolla, M. Mattes

EPFL-STI-IEL-LEMA,
Station 11, CH -1015 Lausanne, Switzerland.
apostolos.sounas@epfl.ch

I. INTRODUCTION

The increased demand for high-quality services in satellite communications leads to the need to operate payload at higher power levels. This fact, combined with the low pressure conditions, makes satellite systems susceptible to the well-known multipactor phenomenon [1]-[3], a RF breakdown discharge that can disturb the electrical performance of the devices. Serious problems may appear, like increase of the noise level, growth of return losses or even the device destruction in case that a corona discharge is caused [4], [5]. Therefore, nowadays, multipaction prediction constitutes a crucial issue in payload designing in order to avoid potential malfunctions of the satellite systems, which entail huge repairing costs. For this reason, the development of software tools that simulate multipaction phenomenon has triggered special interest in recent years [6]-[8].

Among other structures, coaxial cables and connectors are essential parts in a satellite system, which can suffer from multipaction. The problem is mainly met in transitions between the coaxial cables and the connectors, where, due to mechanical tolerances, various gaps between the inner and the outer conductor can appear [9]. A possible RF breakdown in this part of the system will disturb the signal transmission and it will affect the performance of the whole communication system.

In this paper, an efficient engineering tool capable to simulate multipaction phenomenon in coaxial geometries will be presented. The developed method estimates the number of the free electrons between the two conductors as a function of time. Depending on the electrons population trend it can be predicted whether a multipaction event is likely to take place or not. As a main output, the so called multipactor chart is plotted which shows the input power levels that can be safely operated in terms of frequency.

The proposed tool was designed under a general concept. It is not restricted to only common coaxial lines but it can also deal with any configuration that includes a 1D field distribution. Moreover, it offers the possibility of analysing structures that have surfaces with different material properties. This makes it a powerful engineering tool for multipaction analysis in a wide range of structures that can be locally approximated by a 1D configuration.

II. FORMULATION

Model Assumptions

As mentioned in the introduction, a 1D model is used for the study of the multipactor phenomenon in coaxial structures. The free electrons are considered to move along the radial direction between the two conductors under the presence of the applied electric field. This approach is valid in coaxial lines for the fundamental mode, since the electric field is unidirectional, thus, enforcing the radial movement of the electrons. The effect of the magnetic field is not taken into account because of the 1D nature of our technique. However, this can be assumed consistent as a first approximation since the effect of the electric field on the electrons dynamics is much stronger than the corresponding one from the magnetic field.

Regarding the particle's representation, the technique is based on the single electron model [10]. According to this, all the particles are assumed to travel simultaneously with the same speed, composing thus an infinitely thin electron sheet between the two surfaces. Hence, in 1D, only a single effective particle is considered. This particle, also referred to as macro-particle, contains all the information about the total number of free electrons. This does not allow a statistical representation of the multipaction progress and it also neglects any mutual repulsion between electrons. However, it constitutes an efficient technique if only the multipaction onset is to be examined.

Multipactor Algorithm

The algorithm starts with a single electron placed at a random position between the two conductors having a random initial velocity. Afterwards, a numerical integrator is used to simulate the electron's motion based on the Lorentz force that in 1D takes the following form:

$$F = qE(r,t), \tag{1}$$

where $q = -e$ is the electron charge, E the scalar field along the radial direction and r the electron's position at the time t. The equation of motion is solved using the 4th order Runge-Kutta differential scheme that can fairly track the electron's motion until an impact happens. In this case, a Secondary Emission Model (SEM) is used to update the state of the macro-particle after the impact. To this end, the Secondary Emission Yield (SEY) model formulated in [11] has been applied. This model was preferred among others since it takes into account both emitted and reflected electrons as it is shown in Fig. 1. After each impact, the total number of free electrons is calculated as follows:

$$N^i = \prod_{i=1}^{n} \delta^i \tag{2}$$

where i denotes $\delta^i = \delta(u_{imp})$ the ith impact, n is the total number of impacts and $\delta^i = \delta\left(u_{imp}\right)$ is the SEY value calculated for each collision according to the corresponding impact velocity u_{imp}. The operation of the SEM is completed by setting the velocity, or, equivalently, the kinetic energy, of the reemitted effective electron equal to a constant value, usually 4 eV.

The algorithm continues the above procedure until a preselected time period is reached. Depending on the electrons population trend it can be predicted whether multipaction is likely to take place or not. A multipaction chart that shows the susceptibility zones in terms of input power and operation frequency can also be obtained.

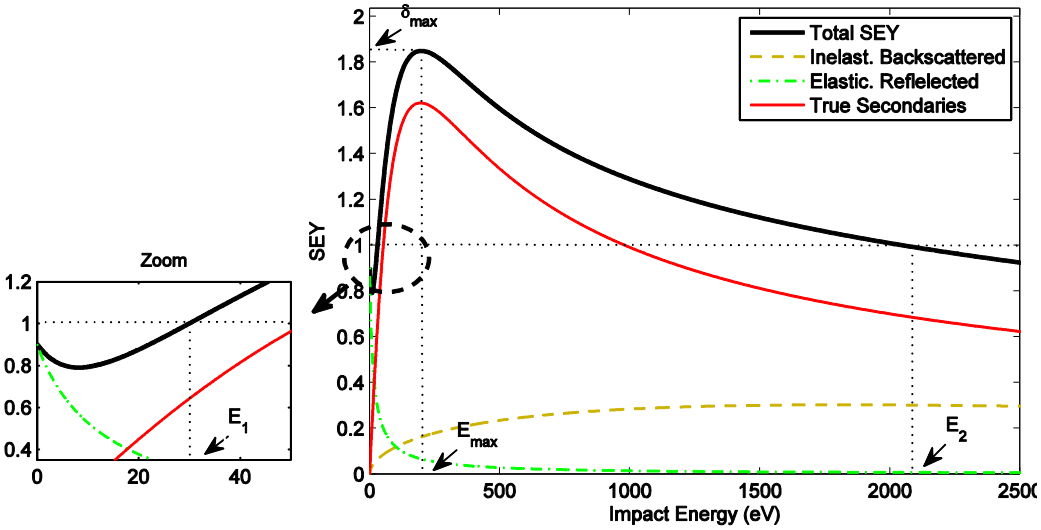

Fig. 1. A typical SEY as it is formulated in [11]. The total SEY results from the contribution of the true secondary, of the inelastically backscattered and of the elastically reflected electrons. As it is shown, the mechanism of the elastically reflected electrons dominates the total SEY in the low impact energy region.

Generalized Concept

Our simulation tool is not restricted to only coaxial lines but is also applicable to any 1D configuration. Since a numerical integrator is employed for tracking the particle's motion the multipaction algorithm is independent from the electric field distribution. To this end, in the above described technique the field between the two surfaces can be given either analytically, if it is possible, or it can be read from an electromagnetic simulation tool. Therefore, our method is able to simulate the multipaction onset in a variety of geometries where the electric field can be locally approximated by

a 1D representation. Additionally, in the proposed approach the two conductors can be characterized by independent material properties. This allows multipaction analysis in structures where any combination between the two surfaces can appear, like in coaxial connectors.

III. NUMERICAL RESULTS

This section presents numerical results obtained by the proposed technique. In the following simulations 1000 time steps per RF period were used in the Runge-Kutta scheme whereas the velocity of the reemitted macro-particle was assumed to be 4 eV. Additionally, Table I includes the SEY parameters that were used for the simulations. The values of E_1, $E_{\max}$ and $\delta_{\max}$ were extracted from [9], [12] whereas the values of $\varepsilon_{0,elast}$ and $\alpha_{inelast}$ from [11].

Table I. SEY properties of different materials applying the model of [11]

	E_1 (eV)	$E_{\max}$ (eV)	$\delta_{\max}$	$\varepsilon_{0,elast}$	$a_{inelasr}$
Silver [11],[12]	30	165	2.22	0.5	8.3×10^{-3}
Copper [11],[12]	25	175	2.25	0.5	7.8×10^{-3}
Alodine [11],[12]	41	180	1.83	0.5	9.8×10^{-3}
Gold [9],[11]	25	288	2.56	0.5	8.3×10^{-3}

Multipactor Chart

First, it is useful to make some comments on the representation of the multipactor chart, that is the main output of our developed algorithm. Fig. 2(a) shows a typical multipactor chart for a coaxial line as it is obtained from our technique. The color intensity represents the total number of the free electrons as it is estimated when the preselected total simulated time is reached. Actually, the absolute values in this chart do not correspond to the real number of the free electrons that will be produced since no saturation mechanisms are taken into account. However, it constitutes a fairly representative measure of the multipaction onset possibility. For a certain value of frequency-gap product, the more intensive the color is, the more risky is the operation of a device in that area. This way of representation was preferred over the classical one with the absolute boundary susceptibility curve since the multipactor effect depends on many parameters that are difficult to be exactly defined.

The multipactor chart itself provides a fast and global view of the structure behavior under multipaction conditions. However, one can have a better aspect by examining the electrons population trend for a selected operation point. Fig. 2(b) shows the population trend for four different cases marked in the multipaction chart. For a proper comparison, the

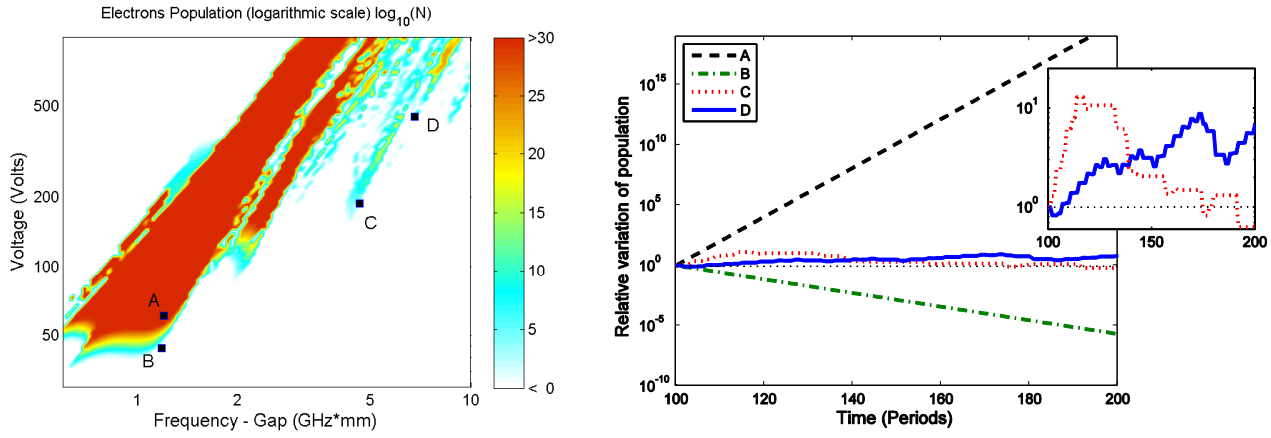

(a) (b)

Fig. 2. (a) A typical multipactor chart as it is obtained from the proposed simulation tool. The color intensity corresponds to the estimated number of free electrons (orders of magnitude) after the maximum simulated time has been reached. (b) Electron population trend after 100 time periods for the four cases marked in the multipactor chart. The y-axis corresponds to the relative variation of electrons number with respect to the population at the 100th period. The data are for a coaxial line of $Z = 50\ \Omega$. Silver material is assumed.

curves indicate the relative number of electrons with respect to the population at the $100th$ period. When the operation point is relatively far from the susceptibility boundaries (cases A and B) there is a clear indication if the multipaction will take place or not. However, in the marginal cases C and D there is an uncertainty regarding the multipaction onset since the population follows an oscillating behavior.

Validation

First, we have validated our simulation tool with some measurements extracted from Woo [13]. The examined structure was a coaxial cable with a characteristic impedance of $Z = 50\,\Omega$, that corresponds to a ratio between the outer and the inner conductor $r_{out}/r_{in} \approx 2.3$. Both electrodes were built using copper. Regarding the multipaction simulation, a preselected number of $N = 200$ time periods $T = 1/f$ was chosen. Fig. 3(a) shows the multipactor chart as obtained with the proposed algorithm in comparison with the Woo measurements that correspond to the multipactor threshold. As it is observed the numerical results follow very well the experimental data. Both lower and upper thresholds are in good agreement with the susceptibility zones except for the very low frequency-gap product region. The sharp shape of the multipaction chart in this area seems to come from the poor statistical representation due to the single electron model. We expect a better agreement in this region by a more proper representation of the statistics which are currently implemented.

Next, we have compared our tool with the method described in [7] for predicting the multipactor threshold in coaxial lines. Comparative results for a sample line made of alodine material are given in Fig. 3(b). A very good agreement between the shape of the susceptibility zones and the threshold from [7] can be noticed for a wide range of the frequency-gap product.

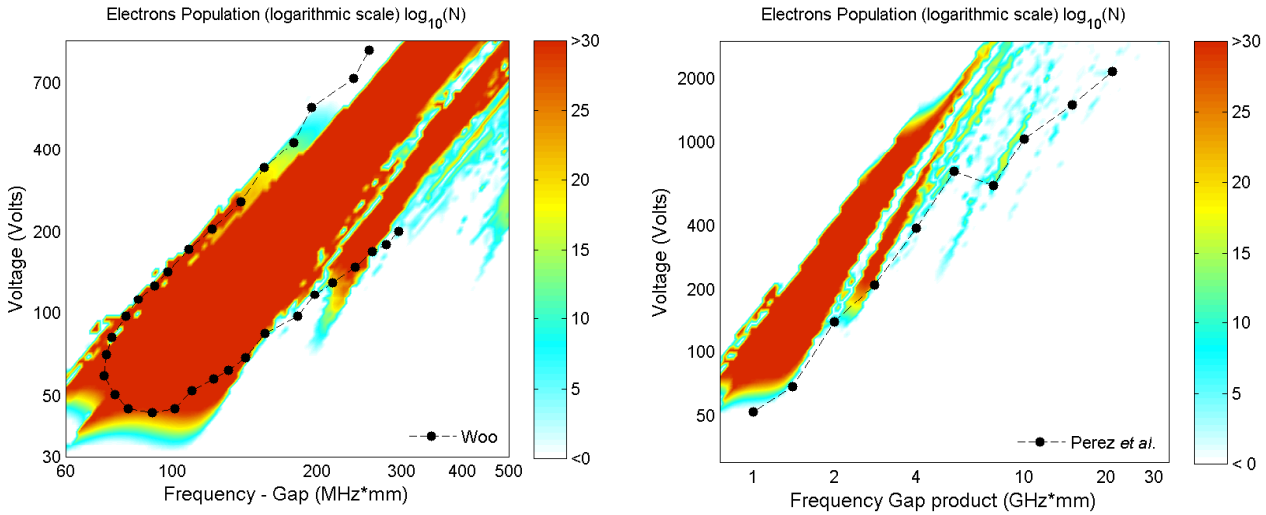

(a) (b)

Fig. 3. Comparative results with (a) Woo experiments [13] for a coaxial line of copper, (b) [7] for a coaxial line of alodine. In both cases the characteristic impedance is equal to $Z = 50\,\Omega$.

Single-Sided Multipactor

Apart from the double-sided multipaction, single-sided discharges are also possible in coaxial geometries [14]. This comes from the fact that the electric field is inhomogeneous and stronger near to the inner conductor causing an average force, the so called Miller or ponderomotive force, that pushes the electrons towards the outer conductor. We have examined single-sided multipaction in two cases, where the coaxial lines are characterized by an impedance of 50 Ω and 100 Ω respectively. Fig. 4 depicts the susceptibility zones where the regions of double- and single-sided multipaction are separated. As it was expected single-sided multipaction mainly appears in the region of high frequency-gap products. Since this area corresponds to larger gaps an electron which is emitted from the outer surface is more probable to come back before it impacts the inner conductor. Additionally, comparing Fig. 4(a) and Fig. 4(b) it is

illustrated that the single-sided mechanism is more evident in coaxial lines with higher characteristic impedance, that is with larger ratio r_{out}/r_{in} .

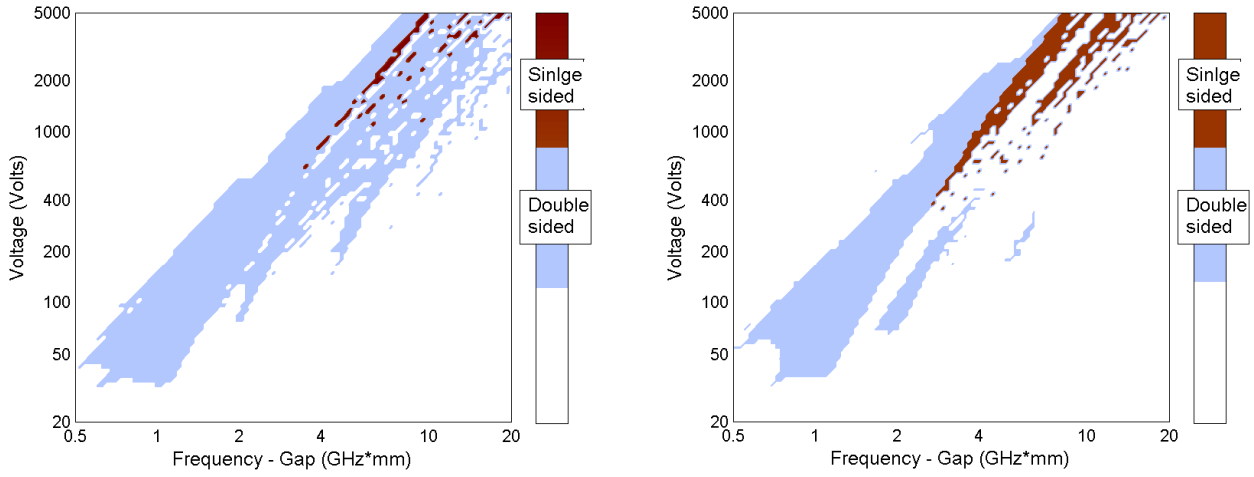

(a) (b)

Fig. 4. Separated regions of double- and single-sided multipaction for a coaxial line of (a) $Z = 50\ \Omega$ and (b) $Z = 100\ \Omega$. In both cases copper material has been considered.

Multipaction in SMA connectors

To show the versatility of the implemented algorithm, we consider a real-world problem in this section: the interesting case of studying the multipaction onset in a SMA connector. Due to mechanical tolerances an air gap between the male and female part can appear when they are mated [9], as it is illustrated in Fig. 5. Under vacuum conditions, this area is possible to be affected by the multipaction phenomenon. Assuming that multipaction is most likely to take place in the central part of the examined gap, we have applied our method on the line *AB* (Fig. 5) where the field is mainly radial. An electromagnetic simulation analysis has been performed using a commercial FEM solver in order to obtain the electric field distribution. It has been found that the field remains almost the same in the frequency range till 18 GHz. As Fig. 6 shows, the field follows a different trend comparing with that one obtained if the structure was approximated as a coaxial line with the same gap voltage. In order to compare results obtained by applying either the realistic field distribution or the corresponding coaxial approximation, simulations have been performed for the both cases. Fig. 7 presents the computed multipaction charts in addition with the threshold of ECSS standardization [12]. As it is shown,

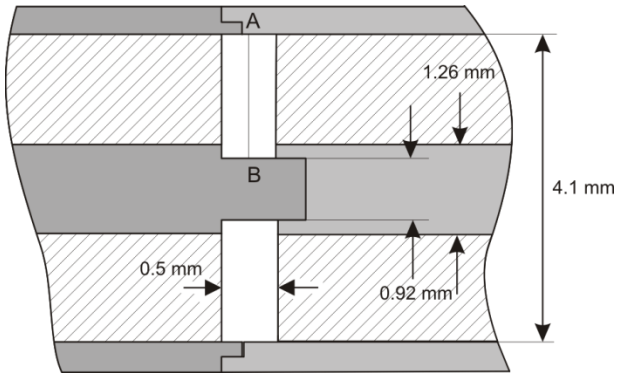

Fig. 5. The geometry of the examined SMA structure. The metallic part is built from gold whereas the dielectric is Teflon PTFE.

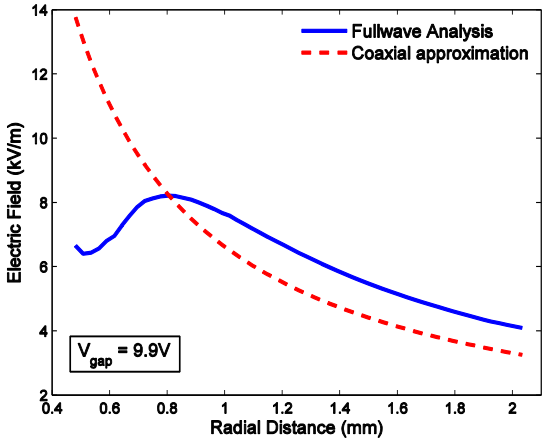

Fig. 6. The electric field along the line AB. The solid line corresponds to the field distribution as it is obtained using a full-wave FEM solver whereas the dashed one is the field as it would be in a coaxial line with the same gap voltage.

the choice of the field distribution has a remarkable effect in the susceptibility zones. The main differences are observed in the frequency range between and 1 and 5 GHz where the coaxial approximation yields susceptibility zones of lower power levels. Moreover, a significant difference in the electrons population in the high frequency region can be observed, too, where, as previously discussed, single-sided multipaction is likely to take place. As Fig. 8 illustrates, the single-sided mechanism is much more intensive in that area when the coaxial approximation is applied, thus, resulting in a less augmentative trend in the electrons population.

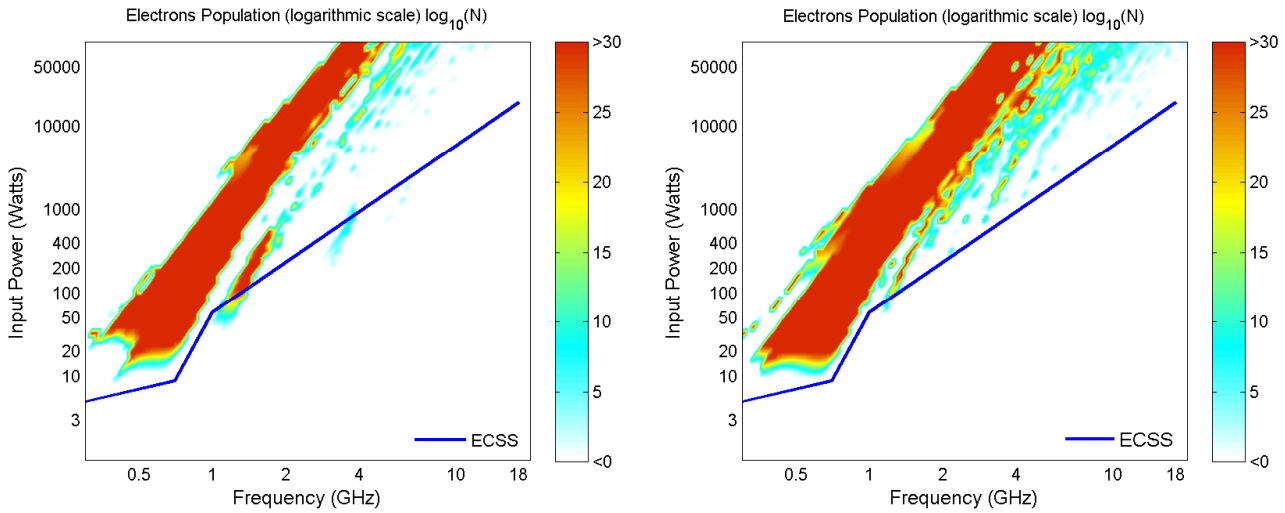

(a) (b)

Fig. 7. Multipaction chart for the geometry of Fig. 5 as it is obtained by applying (a) the field based on the coaxial approximation (b) the field as it is estimated by the full-wave analysis. In both charts, the threshold of ECSS standardization [12] has been added.

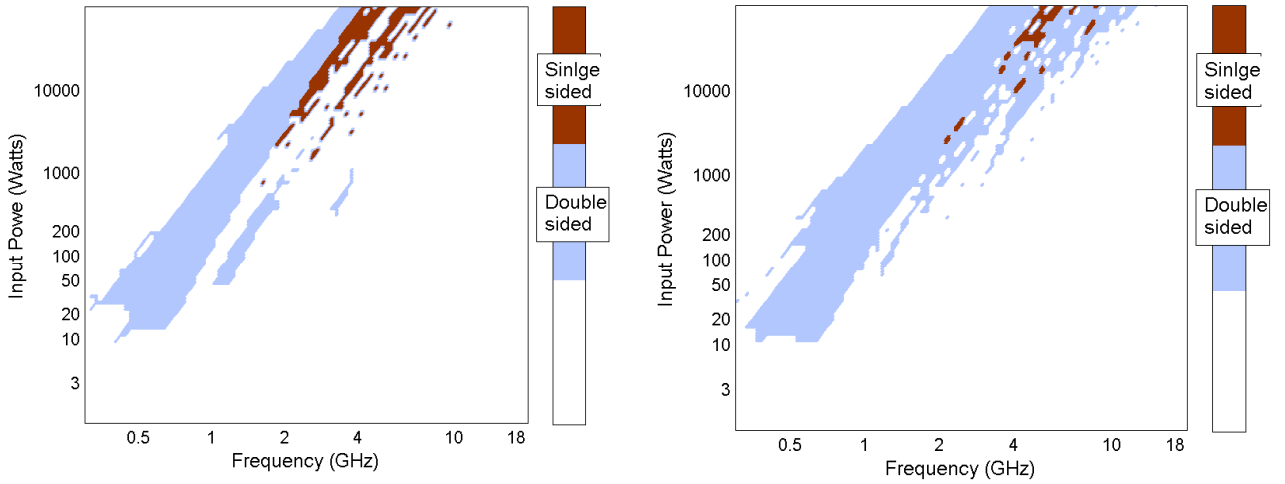

(a) (b)

Fig. 8. Separated regions of double- and single-sided multipaction for the geometry of Fig. 5 as they are obtained by applying (a) the field based on the coaxial approximation (b) the field as it is estimated by the full-wave analysis.

IV. CONCLUSIONS

In this paper, we have described a numerical technique for studying the multipaction effect in 1D configurations and we have presented its application to coaxial geometries. Good agreement with experimental and numerical data has been demonstrated. Additionally, it has been shown that the proposed method can take into account both single- and double-sided multipaction whereas by detecting the zones of these two mechanisms an enriched explanation of the multipaction chart is possible. Beyond that, it offers the possibility for studying the RF breakdown in structures where the field distribution does not take an analytical form. It should be stressed out that the method is not targeted to a rigorous

analysis of the multipaction phenomenon but it is intended as an efficient engineering tool that one can use to have a fast and a realistic view of the multipaction onset in a variety of structures.

Due to its generalized concept, the method offers a lot of possibilities for future extensions. Among them, the statistics of the multipaction phenomenon as well as the space charge effect are currently implemented.

ACKNOWLEDGEMENT

This work has been supported by the Swiss National Science Foundation (SNF) under the project "Modelling microwave-electron interaction in the LHC beam pipe" (SNF contract no. 200021 129661).

REFERENCES

[1] P. T. Farnsworth, "Television by electron Image scanning", *Journal of the Franklin Institute*, vol. 218, pp. 411–444, 1934.

[2] J. Vaughan, "Multipactor", *IEEE Trans. on Electron Devices*, vol. 35, pp. 1172-1180, July 1988.

[3] R. Kishek, Y. Lau, L. Ang, A. Valfells, and R. Gilgenbach, "Multipactor discharge on metals and dielectrics: Historical review and recent theories", *Physics of Plasmas*, vol. 5, pp. 2120–2126, May 1998.

[4] R. Kishek, Y. Y. Lau, "Interaction of Multipactor Discharge and RF Circuit", *Physical Review Letters*, Vol. 75, No. 6, pp. 1218-1221, Aug. 1995.

[5] F. Hohn, W. Jacob, R. Beckmann, and R. Wilhelm. "The transition of a multipactor to a low-pressure gas discharge," *Phys. Plasmas*, 4(4): 940-944, April 1997.

[6] C. Vicente *et al*. "Multipactor breakdown prediction in rectangular waveguide based components", IEEE MTT-S International Microwave Symposium Digest, June 2005.

[7] A. Perez *et al*., "Prediction of Multipactor Breakdown Thresholds in Coaxial Transmission Lines for Traveling, Standing, and Mixed Waves," *IEEE Transactions on Plasma Science*, vol.37, no. 10, pp. 2031-2040, Oct. 2009.

[8] F. Pérez, *et al*. "CEST and MEST: Tools for the simulation of radio frequency electric discharges in waveguides," *Simulation Modelling Practice and Theory* 16(9), pp. 1438-1452, 2008.

[9] "High Power SMA Connectors", ESA Contract No. 20967/07/NL/GLC.

[10] E. Somersalo, P. Ylä-Oijala, D. Proch, and J. Sarvas, "Computational methods for analyzing electron multipacting in RF structures," *Part. Accel*., vol. 59, pp. 107–141, 1998.

[11] J. Lara *et al*., "Multipactor Prediction for On-Board Spacecraft RF Equipment With the MEST Software Tool," *IEEE Transactions on Plasma Science*, vol. 34, no. 2, pp. 476-484, April 2006.

[12] "*Space Engineering – Multipaction Design and Test*," ECSS – E-20-01A, ISSN: 1028-396X, May 2003.

[13] R. Woo, "Multipacting discharges between coaxial electrodes", *J. Appl. Phys.*, vol. 39, p.1528 , 1968.

[14] R. Udiljak, D. Anderson, M. Lisak, V. Semenov, and J. Puech, "Multipactor in a coaxial transmission line. Part I: Analytical study," *Phys. Plasmas*, vol. 14, no. 3, p. 033 508, Mar. 2007.